Chapter

TiO_2 Based Nanomaterials and Their Application as Anode for Rechargeable Lithium-Ion Batteries

Nabil El Halya, Karim El Ouardi, Abdelwahed Chari, Abdeslam El Bouari, Jones Alami and Mouad Dahbi

Abstract

Titanium dioxide- (TiO_2-) based nanomaterials have been widely adopted as active materials for photocatalysis, sensors, solar cells, and for energy storage and conversion devices, especially rechargeable lithium-ion batteries (LIBs), due to their excellent structural and cycling stability, high discharge voltage plateau (more than 1.7 V versus Li^+/Li), high safety, environmental friendliness, and low cost. However, due to their relatively low theoretical capacity and electrical conductivity, their use in practical applications, i.e. anode materials for LIBs, is limited. Several strategies have been developed to improve the conductivity, the capacity, the cycling stability, and the rate capability of TiO_2-based materials such as designing different nanostructures (1D, 2D, and 3D), Coating or combining TiO_2 with carbonaceous materials, and selective doping with mono and heteroatoms. This chapter is devoted to the development of a simple and cost-efficient strategies for the preparation of TiO_2 nanoparticles as anode material for lithium ion batteries (LIBs). These strategies consist of using the Sol–Gel method, with a sodium alginate biopolymer as a templating agent and studying the influence of calcination temperature and phosphorus doping on the structural, the morphological and the textural properties of TiO_2 material. Moreover, the synthetized materials were tested electrochemically as anode material for lithium ion battery. TiO_2 electrodes calcined at 300°C and 450°C have delivered a reversible capacity of 266 mAh g^{-1}, 275 mAh g^{-1} with coulombic efficiencies of 70%, 75% during the first cycle under C/10 current rate, respectively. Besides, the phosphorus doped TiO_2 electrodes were presented excellent lithium storage properties compared to the non-doped electrodes which can be attributed to the beneficial role of phosphorus doping to inhibit the growth of TiO_2 nanoparticles during the synthesis process and provide a high electronic conductivity.

Keywords: Lithium-ion Battery, TiO_2 based materials, Gelation of biopolymers, Sodium alginate, conductivity, Phosphorus doping

IntechOpen

1. Introduction

In recent years, lithium-ion batteries (LIBs) have been established as efficient electrochemical energy storage devices and have become the best choice for electric vehicles (EVs) and mobile phones due to their long cycle life, low self-discharge rate, high working voltage, high power and energy density [1, 2]. Developing and using LIBs can significantly reduce pollution of combustion gas by replacing traditional transportation powered by gasoline with environmentally friendly electric vehicles. Following their success in the transport sector, batteries have recently been considered for grid applications, contributing this to the improvement of the energy efficiency of solar, wind, tidal and other clean energy technologies. LIBs are therefore considered to be an essential element in the building an energy-sustainable economy [3, 4].

Figure 1 present the working principle of LIB; both anodes and cathodes could possess a host structure for Li^+ ions to ensure a good insertion/ disinsertion of these ions during the charge and discharge. The electrolyte is the polypropylene/ polyethylene which contains lithium salts (i.e., $LiPF_6$) in alkyl organic carbonates. The separator, usually Celgard or Whatman, must allow the diffusion of Li^+ ions between the cathode and the anode during the charging and discharging process [5].

The development of large and efficient batteries operating at high potentials necessitates the use of elements that give low an anode intercalation potential. Today, Li^+ is considered to give the best performances and is therefore widely used. In addition to improving the electrochemical characteristics of anodes, researchers are also concerned with the cost and the environmental impact of the materials under development. In general, an ideal anode material must possess the following characteristics [6, 7]:

- High specific surface area offering more lithium insertion channels,
- Good cycling stability and low volume change during Li ion insertion/ desertion process.
- Large pore size for fast Li^+ ion diffusion and good rate capability,

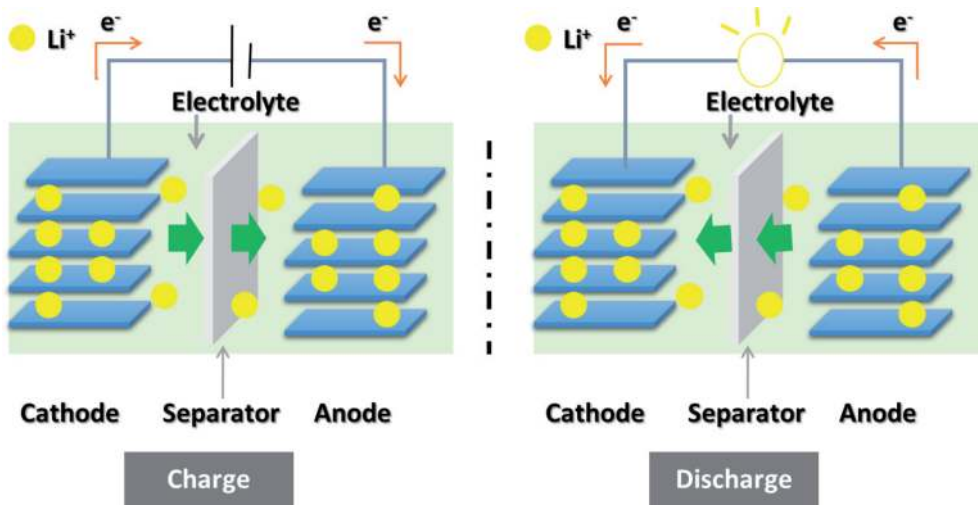

Figure 1.
Working principle of current rechargeable lithium-ion batteries.

- Low internal resistance which allows fast charging and discharging process,
- low lithium ions intercalation potential,
- low price and environmental friendliness.

Most commercial LIBs use transition metals oxides or phosphates such as $LiCoO_2$, $LiFePO_4$ and $LiMnPO_4$, as active materials for the cathode, while, the anode is typically made of graphite. Despite its wide commercial use, graphite suffers from a large volume variation during the charge/ discharge process, a low specific capacity, besides safety concerns. To overcome these concerns, TiO_2 is a promising alternative, as it possess excellent structural and cycling stability, high discharge voltage plateau (more than 1.7 V versus Li^+/Li), high safety, is environmentally friendly, and has a low cost [7, 8]. However, some of the limiting features of this material, including its low electrical conductivity, low capacity and poor rate capability need to be overcome. **Figure 2** shows the potential versus Li/Li^+ and the corresponding capacity density of some potential active anode materials and **Table 1** presents a brief comparison between TiO_2 and other anode active materials.

Several strategies have been developed to improve the capacity, the cycling stability, and the rate capability of TiO_2-based anodes, and are detailed in the next paragraphs.

1.1 Designing different nanostructured TiO_2

1.1.1 One-dimensional nanostructures (1D)

Nanostructured materials, such as nanotubes, nanowires, nanoneedles, nanofibers and nanorods have been designed for high performance anodes. The interesting performance of 1D TiO_2 was demonstrated by different groups; Tammawat and Meethong studied anatase TiO_2 nanofiber as an anode active material in LIBs,

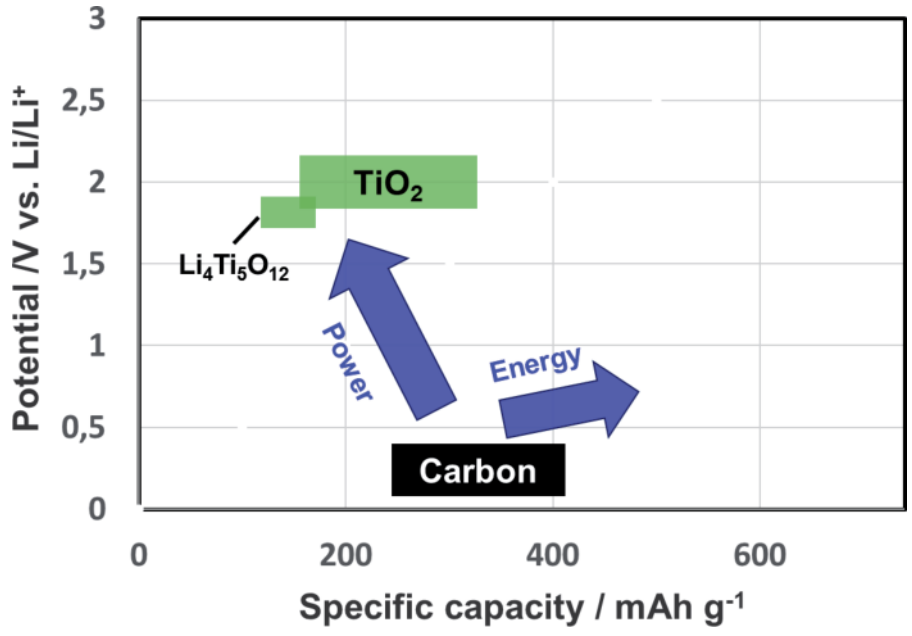

Figure 2.
Potential versus Li/Li^+ and the corresponding specific capacity of some potential active anode materials for lithium ion batteries.

Materials	Theoretical capacity (mAh/g)	Advantages	Drawbacks
Si	4200	High capacity	Poor cycling, large irreversible capacity
Metal oxides	500–1200	Low cost, High capacity	Low electrical conductivity, low capacity retention and coulombic efficiency
Sn	990	Low cost, good electrical conductivity, good safety	Poor cycling
Graphite	372	Low cost, good working potential	High irreversible capacity, low coulombic efficiency
TiO_2	330	Low cost, environmentally friendly, good safety	Low capacity, poor rate capability, low electrical conductivity

Table 1.
Brief comparison between TiO_2 and other anode active materials [5, 9].

showing a high lithium storage capacity with a stable cycle life and a good rate capability [10]. The excellent performances of these nanostructures could be explained by the increased electronic conductivity, the small nanocrystalline size, the large surface area of the nanofibers and the large Li nonstoichiometric parameters. Another study by Armstrong *et al*. demonstrated that TiO_2 nanowires exhibit a high capacity of 305 mAh g^{-1}, which is much higher than the capacity value achieved by the bulk TiO_2 (240 mAh g^{-1}) [11]. These improved results are attributed to the large surface area of the prepared nanowires and the good electronic conductivity.

1.1.2 Two-Dimensional Structure (2D)

Compared with Zero-Dimensional (0D) nanoparticles and One-Dimensional (1D) nanostructures, the 2D nanomaterials can store Li^+ ion in both sides of the structure which offer more exposed surfaces, open charge transport channel for electrolyte penetration and short ion diffusion length [12, 13]. Moreover, the 2D structure is an excellent choice for fast and high lithium storage.

To fabricate 2D TiO_2 materials, significant efforts have been made by several researchers. Li *et al.* have used hydrothermal methods to synthetize mesoporous TiO_2 nanoflakes (10–20 nm) and evaluate their performance as anode. The electrochemical tests showed that the prepared nanoflakes had a good cycling life and a high discharge specific capacity of 261 mAh g^{-1} [14]. Another team demonstrated a simple and green synthesis route of anatase petal-like TiO_2 nanosheets. The obtained TiO_2 materials presented a suitable surface area of 28.4 $m^2 g^{-1}$, which was proposed to be the reason behind the high capacity and the good cycling stability [15].

1.1.3 Three-Dimensional Porous Structure (3D)

In recent years, 3D porous structure materials have attracted much attention, due to their high porosity, high specific surface area, and low bulk density [16, 17]. Gerbaldi et al. synthesized highly crystalline, nonordered mesoporous anatase TiO_2 with excellent rate capability and cycling stability after prolonged cycling [18, 19]. Lou et al. demonstrated a significantly improved lithium storage capability of TiO_2 hollow spheres and sub-microboxes, together with a high specific capacity, an excellent rate capability, and a long-term cycling stability [20, 21].

1.2 Coating or combining TiO_2 with carbonaceous materials

To improve the electrochemical performance of TiO_2 materials, carbon coating was used in order to reduce the charge transfer resistance, improve the Li^+, buffer the large volume changes during lithium insertion/extraction, enhance electron transport and prevent the aggregation of active materials [9–22, 23]. Xia *et al.* have reported a carbon-coated TiO_2 anode material with an enhanced electronic conductivity and a low volume expansion during prolonged cycling [24]. In a different study, chemical vapor deposition was used to synthesize TiO_2/CNTs composites, exhibiting a high specific capacity and a long-term cycling stability [25]. This study demonstrated that the enhanced electrochemical performance of this material is due to the structural stability and the efficient conductive network of the TiO_2 particles offered by CNTs. Etacheri *et al.* mixed TiO_2 with graphene and the synthetized hybrid materials exhibited a high specific capacity, an improved capacity retention and a good rate capability, in comparison with the physical mixture of TiO_2 and reduced graphene oxide [26].

1.3 Selective doping with mono and heteroatoms

To improve the intrinsic conductivity and form more open channels and active sites for Li^+ transport, doping with cationic or anionic dopants has been shown to be advantageous [27, 28]. Liu *et al.* evaluated the performance of Ti^{3+} doped TiO_2 nanotube arrays as anode material for LIBs showing an enhanced lithium ion storage performance with an initial discharge capacity of 101 mAh g^{-1} at a high current density of 10 A g^{-1} [29]. Furthermore, Sn-doped TiO_2 nanotubes were synthetized by Kyerematenge and coworkers delivering higher capacity values compared to non-doped TiO_2 nanotubes [30]. Otherwise, TiO_2 materials with improved specific capacities were synthesized, by other researchers, using B and N and doping elements [31, 32].

In the following chapter, simple and cost-efficient strategies for the preparation of TiO_2 nanoparticles as anode material for LIBs are discussed. These strategies consist of using the Sol–Gel method, with a sodium alginate biopolymer as a templating agent, and studying the influence of the calcination temperature and the phosphorus doping on the structural, the morphological, the textural and the electrochemical properties of TiO_2 material.

2. Impact of calcination temperature on TiO_2 as anode for rechargeable Lithium-ion batteries

Our group has reported the synthesis of anatase TiO_2 as an anode material of LIBs by a facile synthesis method using a biopolymer as a templating agent. In order to stress the effect of the calcination temperature on the structural, morphological, textural and the electrochemical performances, two heating temperatures were selected: 300°C and 450°C [33]. Titanium dioxide was prepared by a sol–gel method. Sodium alginate powder (1 g) was dissolved by magnetic stirring in 100 mL of distilled water until a gel was formed. This gel was added dropwise to a 100 mL solution of titanium (IV) isopropoxide (0.32 M) and left under stirring for 3 h at room temperature. The obtained solid was collected by centrifugation, washed with distilled water, dried at 70°C overnight and calcined at 300°C and 450°C.

Concerning the structural, textural and morphological observations, all analysis technics resulted in the formation of a pure anatase TiO_2 with aggregated

spherical particles. In fact, **Figure 3a** shows that the unannealed sample present an amorphous like structure, while the diffraction spectra recorded for TiO_2–300 and TiO_2–450 materials are clearly crystalline. The Raman spectroscopy, **Figure 3b**, confirmed these findings by the presence of three vibration peaks at 632, 508, and 390 cm^{-1}, attributed to Eg, A1g, and B1g modes, respectively, characteristic of TiO_2 anatase phase [34–36].

For the morphological characterization of TiO_2 particles, Scanning Electron Microscopy (SEM) was used. This is shown in **Figure 4**, where the shapes of the TiO_2–300 and the TiO_2–450 particles are spherical, with an inhomogeneous particles' size distribution (nano and submicrometric spherical particles). EDX spectroscopy demonstrated, on the other hand, the uniform distribution of Titanium and oxygen.

BET was used to confirm the effect of the calcination temperature on the average pore sizes, resulting in the respective value of 4.4 and 6.0 nm for TiO_2–300, and

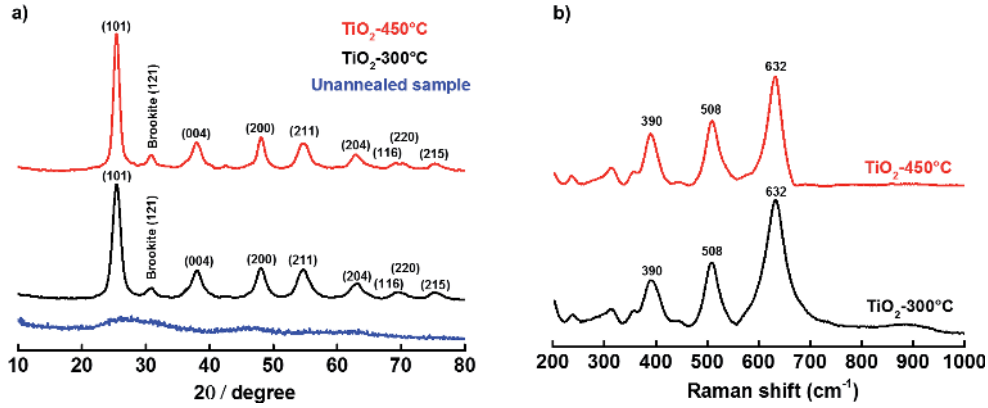

Figure 3.
(a) XRD patterns and (b) Raman spectra of TiO_2material obtained at 300°C (black) and 450°C (red).

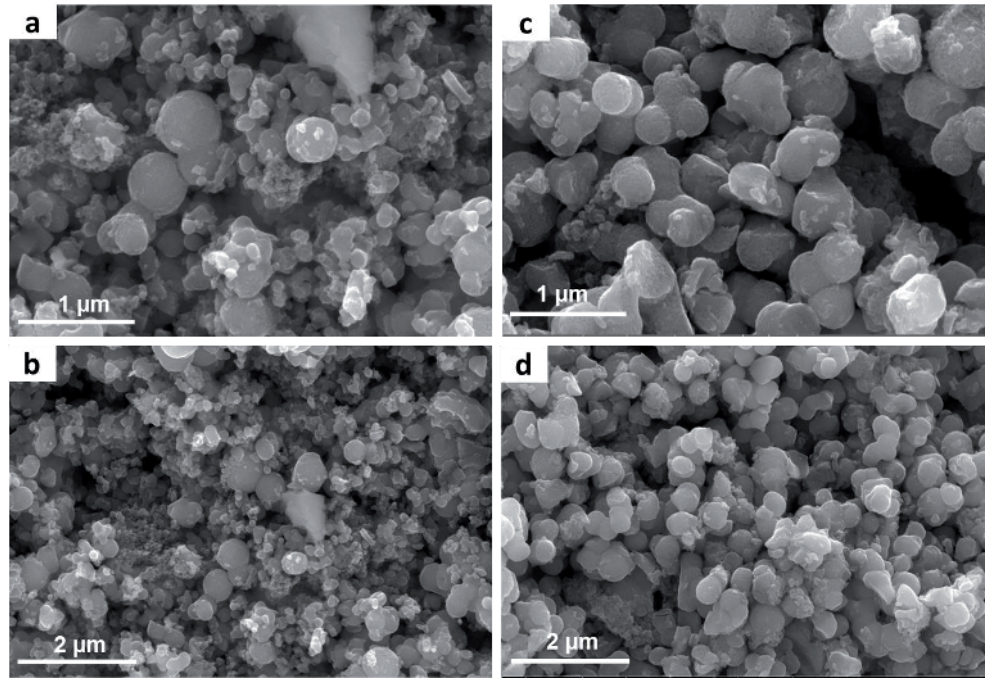

Figure 4.
SEM images of TiO_2 materials calcined at (a, b) 300°C and (c, d) 450°C.

TiO_2–450 (**Figure 5**). Both samples were highly porous, which enhances the surface activity for Li^+ storage and facilitates the liquid electrolyte penetration [33].

In order to evaluate the electrochemical performances of TiO_2–300 and TiO_2–450 electrodes, the charge/discharge tests, cyclic voltammetry, Operando XRD of the TiO_2 electrodes were carried out. The charge/discharge profiles of the two electrodes at a current rate of 0.1C are illustrated in the **Figure 6**. The existence of the cathodic/anodic plateaus located at ~ 1.7 V (lithiation process) and 1.9 V (delithiation process) are characteristic of the TiO_2 anatase polymorph; tetragonal anatase TiO_2 for the non lithiated TiO_2 and orthorhombic $Li_{0.5}TiO_2$ for the Li-rich phase [37, 38]. Besides, the initial reversible capacity of the two electrodes was 266 and 275 $mAh{\cdot}g^{-1}$ for TiO_2–300 and TiO_2–450, respectively. TiO_2–300 and TiO_2–450 electrodes demonstrated a coulombic efficiency (CE) of 70% and 75% in the first cycle and a CE higher than 95% in the other cycles, respectively. From the potential

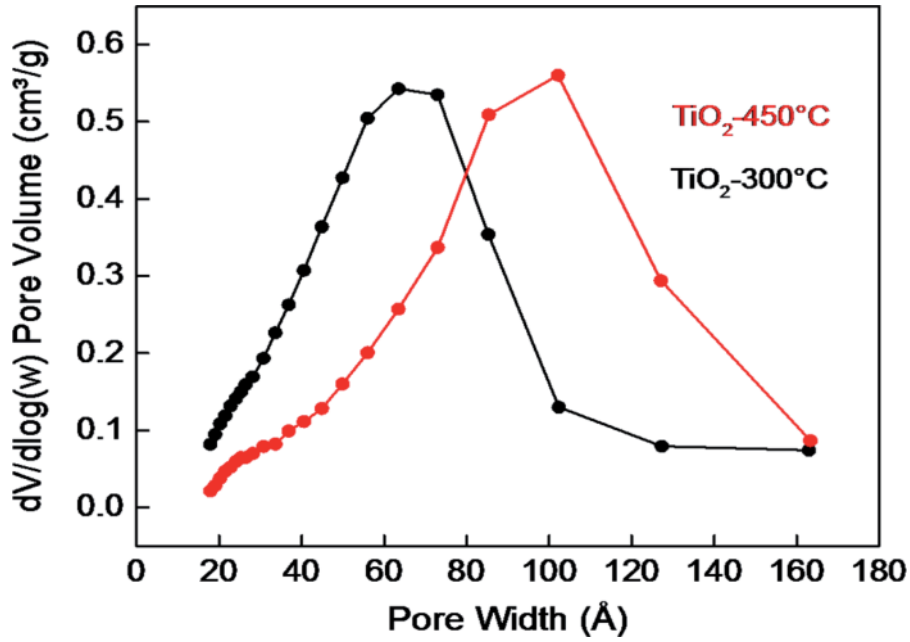

Figure 5.
The pore size distribution curves: (black) TiO_2–300°C, (red) TiO_2–450°C.

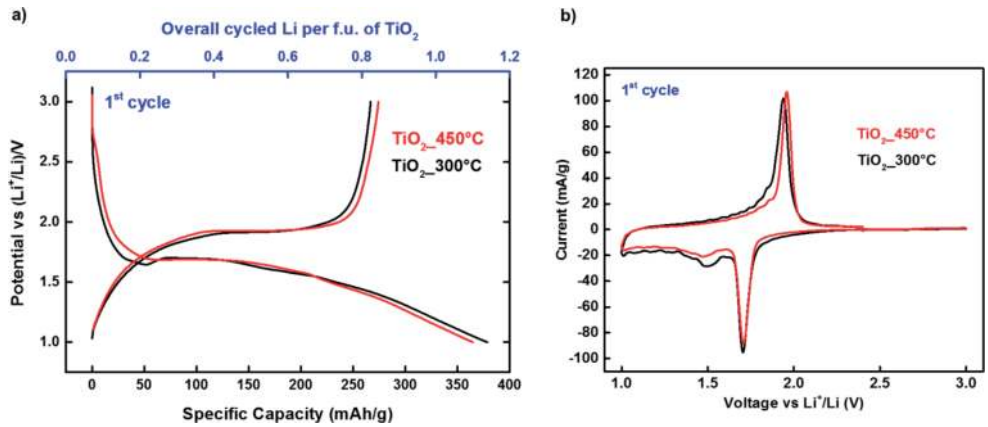

Figure 6.
(a) First charge/discharge profiles of TiO_2electrodes calcined at 450°C (red curve) and at 300°C (black curve) cycled between 3.0 and 1.0 V versus Li/Li^+ at C/10 current rate, (b) cyclic voltammograms of the firstcycle scanned at 0.02 mV s^{-1}.

vs. capacity profile, it is clearly observed that increasing the synthesis temperature from 300 to 450°C has no obvious impact on the cycling process since this profile is very similar.

Concerning the Cyclic voltammetry tests of the as-prepared electrodes (**Figure 6**), there are a pair of reduction/oxidation peaks at ~ 1.7 and 1.9 V for both materials, which could be attributed to the Li-ion intercalation/

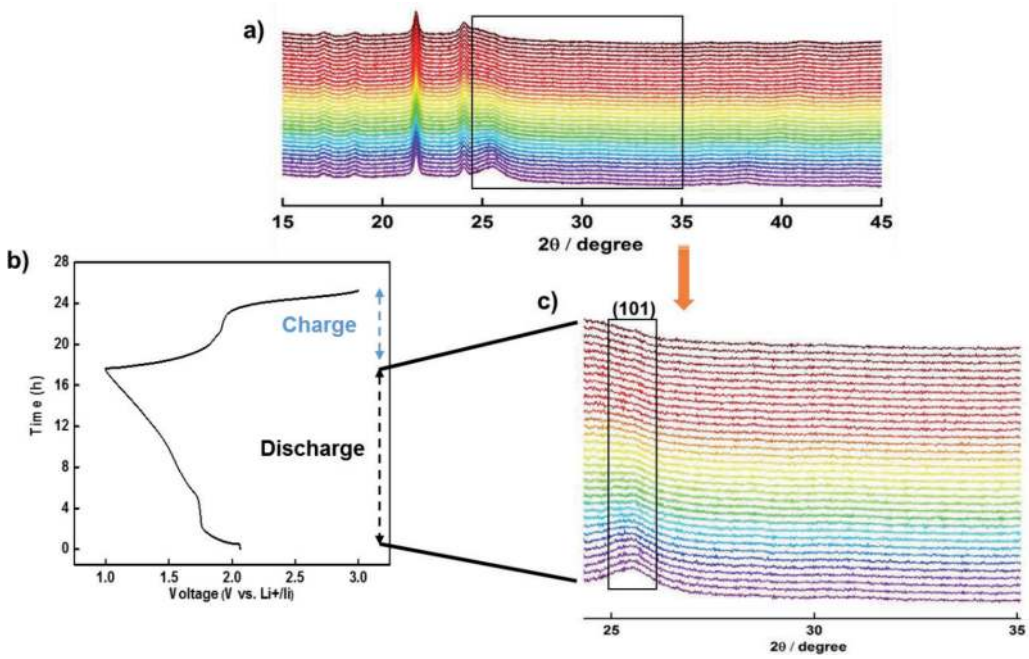

Figure 7.
(a) Operando XRD patterns of TiO_2during the 1st discharge from 3.0 to 1.0 V, (b) 1st discharge/charge galvanostatic data at 0.025C currentrate, (c) the 2Θ region from 24° to 35° showing the disappearance of the (101) reflection peak.

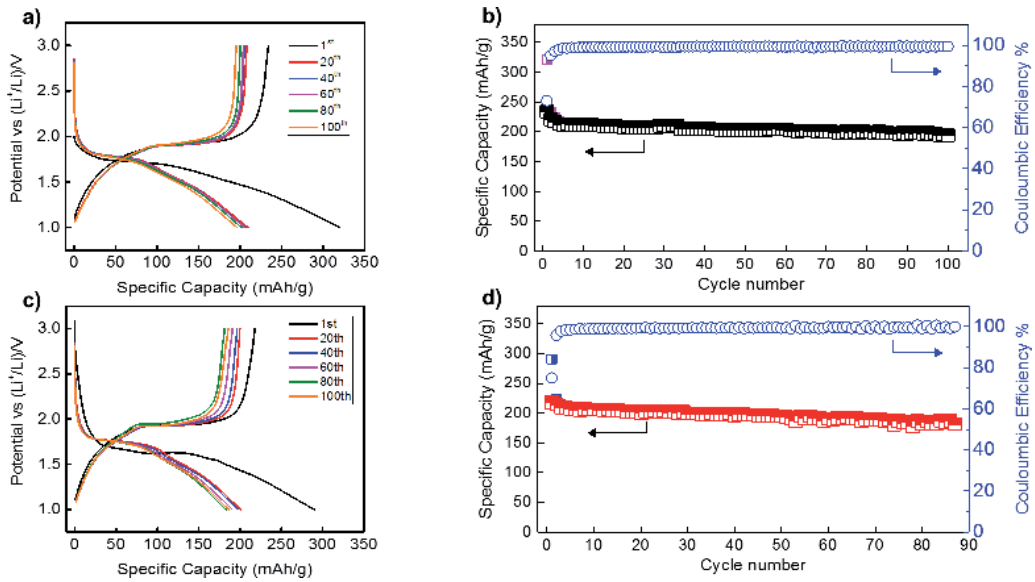

Figure 8.
Galvanostatic discharge/charge curves vs. $Li/Li^+$of (a) TiO_2–300 and (c) TiO_2–450 cycled at a rate of 0.1 C.Cycling performance and coulombic efficiency of (b) TiO_2–300 and (d) TiO_2–450 electrodes cycled between 3.0 and 1.0 V versus Li/Li^+ at 0.1 C current rate.

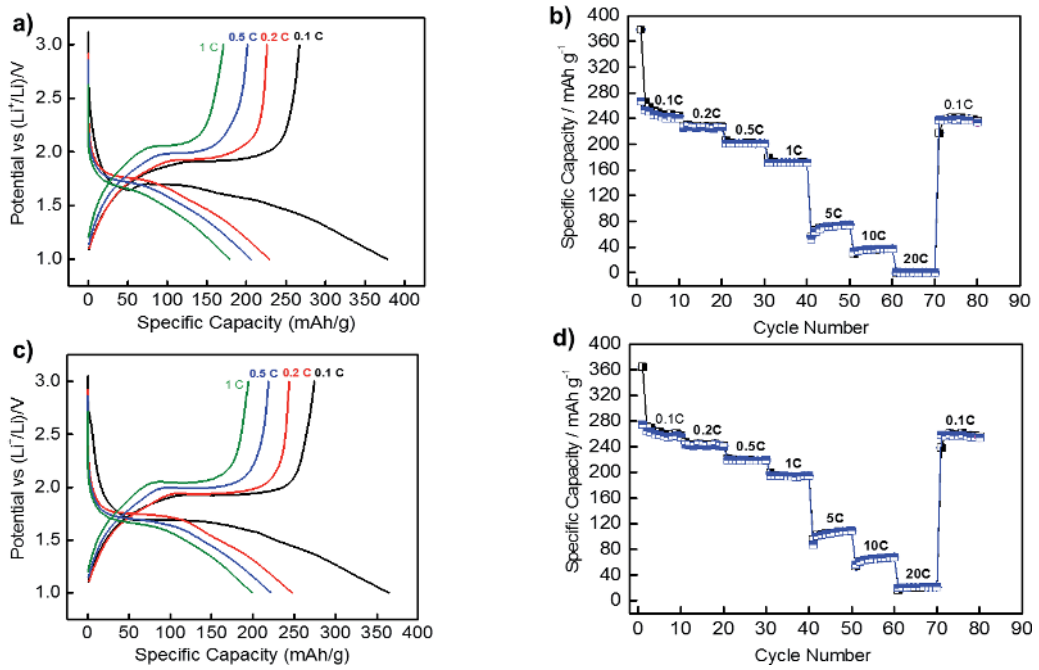

Figure 9.
Galvanostatic charge/discharge profiles at different rates of (a) TiO_2–300 and (c) TiO_2–450, rate capability of (b) TiO_2–300 and (d) TiO_2–450 electrodes at variant current rates from 0.1 C to 20 C (1C = 336 mA g^{-1}).

deintercalation in an anatase TiO_2 lattice (Ti^{4+} reduction/oxidation). The cathodic/anodic peaks were in accordance with the galvanostatic discharge/charge profiles.

In order to follow the structural evolution of the anatase TiO_2 during the lithiation process, an operando XRD measurement during the discharge/charge of the TiO_2–300°C electrode was carried out. As shown in **Figure 7**, the (101) reflection peak characteristic of the anatase phase disappeared during the insertion process, which means that the starting material has been successfully lithiated.

The capacity retention of the two materials is presented in **Figure 8**. After 100 cycles, TiO_2–300 and TiO_2–450 electrodes showed an excellent capacity retention of 88% and 85%, respectively. **Figure 9** presents the rate capabilities of TiO_2 materials evaluated at different current rates at 1.0–3.0 V voltage range. The electrodes were discharged down to 1.0 V and recharged up to 3.0 V at different constant current density from 0.1 to 20 C (1 C = 336 mA g^{-1}). It is clearly observed that the reversible capacity declined gradually with the increase of the current, but still exceeds 73 mAh g^{-1} even at a rate of 5. These excellent electrochemical properties can be explained by the nanoparticle's aspect of TiO_2 prepared by biopolymers gelation method.

3. Impact of phosphorus doping on TiO_2 as anode for Lithium-ion batteries

Another study by our group have evaluated also the impact of phosphorus doping on the electrochemical performances of TiO_2 as anode material for lithium ion batteries. The phosphorus doped TiO_2 was synthesized using a simple and eco-friendly synthesis method, in which titanium tetra-isopropoxide was used as a titanium precursor and sodium alginate as a complexing agent. The effects of P-doping on the crystal structure, morphology and lithium insertion mechanism

were investigated and compared with the undoped TiO_2. Moreover, the P-TiO_2 was tested electrochemically as anode material.

Concerning the synthesis process, TiO_2 and P-TiO_2 materials were synthetized via a gelation of biopolymers, following the synthesis technic proposed by El Ouardi *et al.* and using phosphoric acid as the phosphorus precursor. To prepare the working electrode, black carbon, PVDF and an active material were mixed in a 7:2:1 wt. ratio. The active material of the first electrode contained pure TiO_2 while the second contained TiO_2 doped at 2% phosphorus.

To identify the crystal structures of TiO_2 and P-TiO_2, XRD was carried out and the results are shown in **Figure 10a**. As it can be seen in the diffractograms, the diffraction peaks are centered at 25.3°, 37.9°, 48.1°, 54.7°, 55.0°, 62.7°, 68.9°, 75.04° and 83.0°. These are attributed to the (101), (004), (200), (105), (211), (204), (116), (215) and (312) diffraction planes of anatase TiO_2, respectively, indicating that the crystal phase of TiO_2 remained after phosphorylation treatments [39–41]. At 2θ = 30.7° there is a small peak (*) for the undoped sample, which can be attributed to the existence of the brookite phase, (121) formed during the synthesis [42]. No diffraction peaks that could be attributed to impurities are found in the XRD patterns of TiO_2 and P-TiO_2, suggesting that the sol–gel method can give highly purified anatase TiO_2 products. For the Raman spectra (**Figure 10b**), the obtained bands at 198, 400, 518, and 641 cm^{-1} represent the Raman active modes of anatase TiO_2. These results prove that the prepared nanoparticles have an anatase structure; the non-doped TiO_2 sample contained particles with uniform sizes and homogeneous granular surface, while the P-TiO_2 samples remained unchanged. The energy

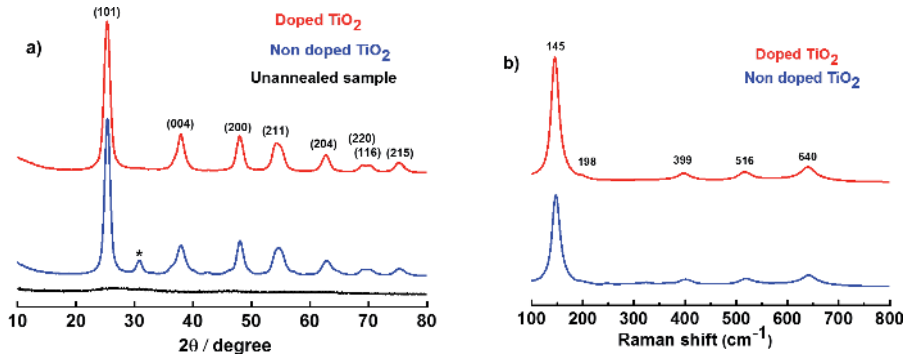

Figure 10.
(a) XRD patterns and (b) Raman spectra of non-doped TiO_2(bleu) and P doped TiO_2 (red) materials obtained at 450°C.

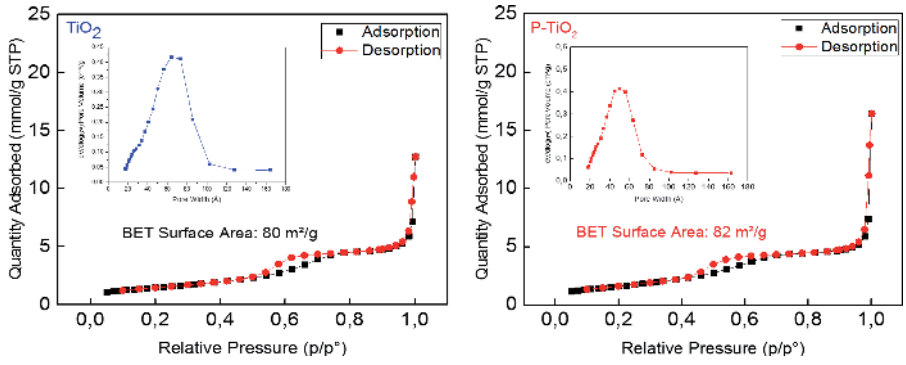

Figure 11.
Nitrogen adsorption–desorption isotherm curves and the pore size distribution curves of non-doped and P doped TiO_2materials obtained at 450°C.

dispersive X-ray (EDX) spectroscopic data of the P-doped TiO_2 demonstrate the uniform distribution of Ti, O and P with no other impurity elements.

The Brunauer–Emmett Teller (BET) method from N_2 adsorption and desorption isotherms carried out at 77 K (**Figure 11**) showed that both materials presented typical IV adsorption/desorption isotherms with mesoporous structures. Besides, both materials exhibited very similar BET surface, pore size distribution and mesopore diameter. For the absorbance measurement, UV-V spectroscopy showed that the phosphorus doping extended the wavelength response range of TiO_2 into the visible-light region (**Figure 12**). Moreover, the band gap of TiO_2 and P-TiO_2 was 2.90 and 2.87 eV, respectively. This result shows the effect of phosphorus doping to reduce the band gap and improve the electrotonic conductivity of TiO_2 [43–45].

Concerning the electrochemical tests, the charge/discharge curves (**Figure 13**) show the presence of two plateaus at 1.9 V and 1.7 V for both materials representing

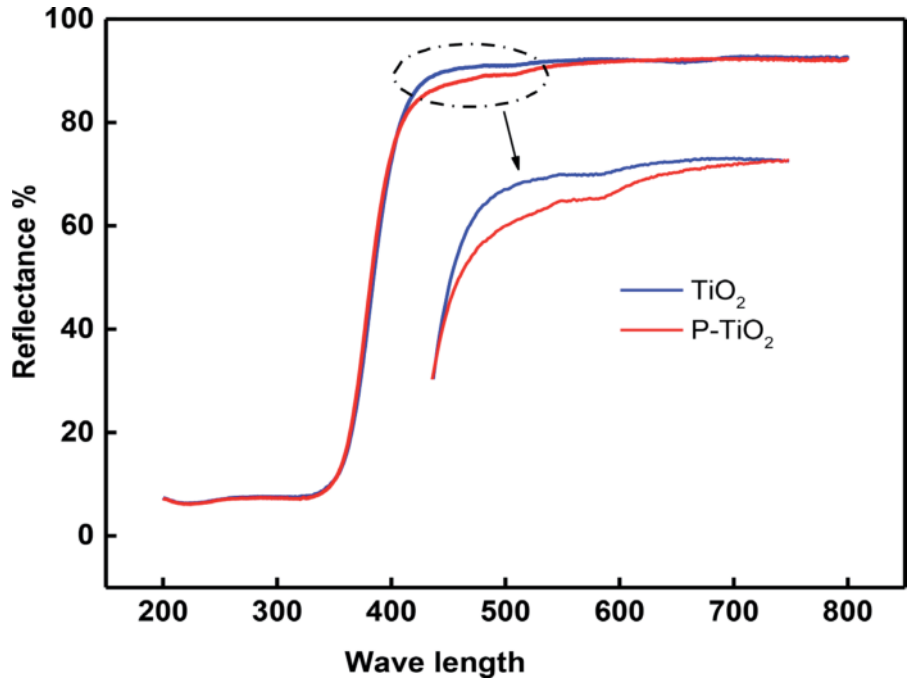

Figure 12.
UV-V spectra of non-doped TiO_2 (bleu) and P doped TiO_2 (red) materials obtained at 450°C.

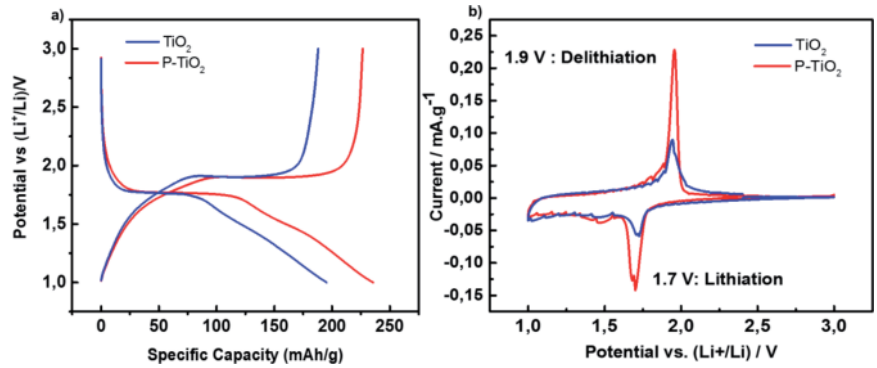

Figure 13.
(a) First charge/discharge profiles of TiO_2 (bleu curve) and P-TiO_2 (red curve) electrodes calcined at 450°C cycled between 3.0 and 1.0 V versus Li/Li^+ at C/10 current rate, (b) cyclic voltammograms of the first cycle scanned at 0.02 mV s^{-1}.

cathodic and anodic peaks of anatase TiO_2 nanoparticles, respectively. This charge/discharge process has shown also a good irreversible capacity which does not exceed 10 mAh/g for both materials. For the polarization, P-TiO_2 has shown improved characteristics compared to non-doped TiO_2. This result could be attributed to the improved electronic conductivity.

Cyclic voltammetry technique was used to study the insertion/extraction properties of lithium ions from the prepared electrodes in the 1.0 and 3.0 V potential window with a scanning speed of 0.02 mV s^{-1}. As it can be seen in **Figure 13**, there are two cathodic (reduction peak I < 0) / anodic (oxidation peak I > 0) peaks at 1.7 and 1.9 V, respectively, attributed to the insertion / extraction of lithium ions in the TiO_2 nanoparticles. This result is with agreement with the galvanostatic discharge/charge profiles.

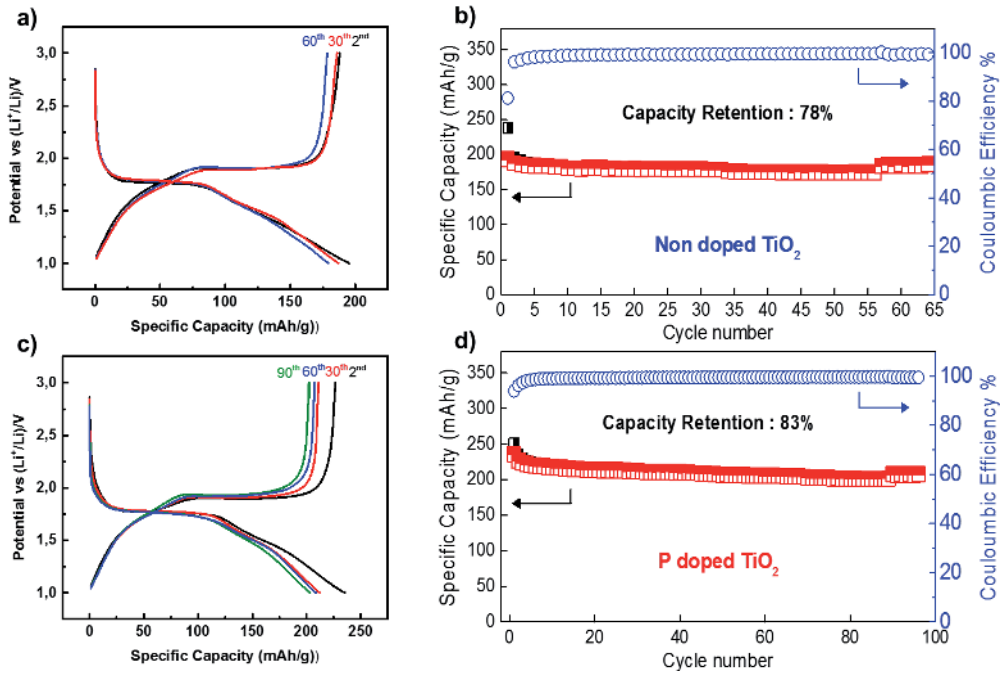

Figure 14.
Galvanostatic discharge/charge curves vs. Li/Li^+ of (a) P doped TiO_2 and (c) non-doped TiO_2 cycled at a rate of 0.1 C. cycling performance and coulombic efficiency of (b) P doped TiO_2 and (d)non-doped TiO_2 electrodes cycled between 3.0 and 1.0 V versus Li/Li^+ at 0.1 C current rate.

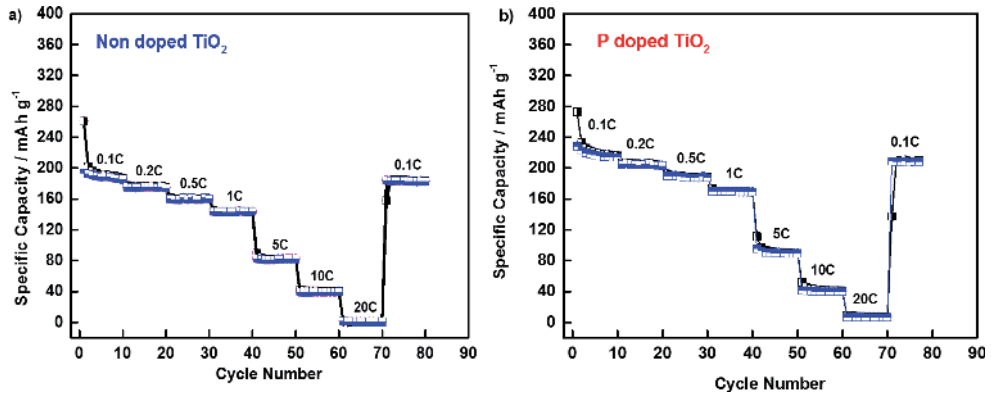

Figure 15.
Rate capability of (a) non doped TiO_2 and (b) P doped TiO_2 electrodes at variant current rates from 0.1 C to 20 C (1C = 336 mA g^{-1}).

For the cycling stability, **Figure 14** prove the excellent coulombic efficiency (about 100%) for both TiO_2 and P-TiO_2 electrodes. Besides, these electrodes showed a capacity retention of 78% after 70 cycles and 83% after 90 cycles, respectively. The reason behind these improved electrochemical properties for P-TiO_2 can be the smaller TiO_2 particle size which permits fast lithium insertion / disinsertion process.

Figure 15 present the rate capabilities of TiO_2 and P-TiO_2 evaluated at different current rates at 1.0–3.0 V voltage range. The electrodes were discharged down to 1.0 V and recharged up to 3.0 V at different constant current density from 0.1 to 20 C (1 C = 336 mA g^{-1}). It is clearly observed that the reversible capacity declined gradually with the increase of the current for both materials, but it still exceeds 80 mAh g^{-1} for non-doped TiO_2 and 98 mAh g^{-1} for P doped TiO_2 even at a rate of 5 C. The capacity at 0.1C rate after 70 cycles was recovered to about 185 mAh g^{-1} for non-doped TiO_2 and 213 mAh/g for P doped TiO_2 after 90 cycles. Thus, indicating the high stability of the anatase TiO_2 nanoparticles and confirming the better performance of P-TiO_2 compared to TiO_2.

4. Conclusion

In summary, this chapter show the huge interest in the development and improvement of TiO_2 as anode for high performance rechargeable lithium ion batteries. Several strategies have been developed to improve the conductivity, the capacity, cycling stability, and rate capability of this material, such as designing different nanostructured (1D, 2D and 3D), Coating or combining TiO_2 with carbonaceous materials, and Selective doping with mono and heteroatoms.

Biopolymer gelation is a simple and economically favorable approach for the preparation of TiO_2 nanoparticles. This method that consists of using the Sol–Gel method with a sodium alginate biopolymer as a templating agent showed enhanced performances in comparison with other synthesis techniques. In fact, the prepared TiO_2 electrodes displayed a high specific capacity above 275 mAh g^{-1} and excellent cycling stability with over 85% capacity retention after 100 cycles. Besides, combining phosphorus doping with this synthesis strategy demonstrated an important discharge capacity of 200 mAh g^{-1} after 90 cycles under C/10 current rate and has an excellent rate performance. The improved electrochemical performance can be explained based on the P-TiO_2 particles size and band gap modifications upon doping proved by UV-V measurement.

Finally, from this chapter, we can conclude that the use of TiO_2-based materials as anode for commercial lithium ion batteries requires more efforts to overcome the problems encountered, especially the low electrical conductivity, the low energy density, the poor cycling life and the low efficiency.

Acknowledgements

The authors wish to acknowledge Office Chérifien des Phosphates (OCP S.A.) for financial support.

Author details

Nabil El Halya[1], Karim El Ouardi[1,2], Abdelwahed Chari[1], Abdeslam El Bouari[2], Jones Alami[1] and Mouad Dahbi[1*]

1 Materials Science, Energy, and Nano-Engineering Department, Mohammed VI Polytechnic University, Ben Guerir, Morocco

2 Laboratory of Physic-Chemical of Applied Materials, Sciences Faculty of Ben M'sik, Hassan II University Casablanca, Morocco

*Address all correspondence to: mouad.dahbi@um6p.ma

IntechOpen

References

[1] Z. Yang *et al.*, "Nanostructures and lithium electrochemical reactivity of lithium titanites and titanium oxides: A review," *J. Power Sources*, vol. 192, no. 2, pp. 588-598, 2009, doi: 10.1016/j.jpowsour.2009.02.038.

[2] L. Jabbour, R. Bongiovanni, D. Chaussy, C. Gerbaldi, and D. Beneventi, "Cellulose-based Li-ion batteries: A review," *Cellulose*, vol. 20, no. 4, pp. 1523-1545, 2013, doi: 10.1007/s10570-013-9973-8.

[3] P. Xiong, L. Peng, D. Chen, Y. Zhao, X. Wang, and G. Yu, "Two-dimensional nanosheets based Li-ion full batteries with high rate capability and flexibility," *Nano Energy*, vol. 12, pp. 816-823, 2015, doi: 10.1016/j.nanoen.2015.01.044.

[4] D. Ma, Z. Cao, and A. Hu, "Si-based anode materials for li-ion batteries: A mini review," *Nano-Micro Lett.*, vol. 6, no. 4, pp. 347-358, 2014, doi: 10.1007/s40820-014-0008-2.

[5] S. Goriparti, E. Miele, F. De Angelis, E. Di Fabrizio, R. Proietti Zaccaria, and C. Capiglia, "Review on recent progress of nanostructured anode materials for Li-ion batteries," *J. Power Sources*, vol. 257, pp. 421-443, 2014, doi: 10.1016/j.jpowsour.2013.11.103.

[6] L. Bai *et al.*, "A sandwich structure of mesoporous anatase TiO2 sheets and reduced graphene oxide and its application as lithium-ion battery electrodes," *RSC Adv.*, vol. 4, no. 81, pp. 43039-43046, 2014, doi: 10.1039/c4ra04979a.

[7] X. Li, Y. Zhang, T. Li, Q. Zhong, H. Li, and J. Huang, "Graphene nanoscrolls encapsulated TiO2 (B) nanowires for lithium storage," *J. Power Sources*, vol. 268, pp. 372-378, 2014, doi: 10.1016/j.jpowsour.2014.06.056.

[8] J. Jin *et al.*, "Design of new anode materials based on hierarchical, three dimensional ordered macro-mesoporous TiO2 for high performance lithium ion batteries," *J. Mater. Chem. A*, vol. 2, no. 25, pp. 9699-9708, 2014, doi: 10.1039/c4ta01775g.

[9] F. Paquin, J. Rivnay, A. Salleo, N. Stingelin, and *C. Silva*, "Multi-phase semicrystalline microstructures drive exciton dissociation in neat plastic semiconductors," *J. Mater. Chem. C*, vol. 3, pp. 10715-10722, 2015, doi: 10.1039/b000000x.

[10] P. Tammawat and N. Meethong, "Synthesis and characterization of stable and binder-free electrodes of TiO2 nanofibers for li-ion batteries," *J. Nanomater.*, vol. 2013, 2013, doi: 10.1155/2013/413692.

[11] A. R. Armstrong, G. Armstrong, J. Canales, R. García, and P. G. Bruce, "Lithium-ion intercalation into TiO2-B nanowires," *Adv. Mater.*, vol. 17, no. 7, pp. 862-865, 2005, doi: 10.1002/adma.200400795.

[12] T. Hu *et al.*, "Flexible free-standing graphene-TiO 2 hybrid paper for use as lithium ion battery anode materials," *Carbon N. Y.*, vol. 51, no. 1, pp. 322-326, 2013, doi: 10.1016/j.carbon.2012.08.059.

[13] Y. Liu, W. Wang, H. Huang, L. Gu, Y. Wang, and X. Peng, "The highly enhanced performance of lamellar WS2 nanosheet electrodes upon intercalation of single-walled carbon nanotubes for supercapacitors and lithium ions batteries," *Chem. Commun.*, vol. 50, no. 34, pp. 4485-4488, 2014, doi: 10.1039/c4cc01622j.

[14] T. D. Nguyen-Phan *et al.*, "Uniform distribution of TiO 2 nanocrystals on reduced graphene oxide sheets by the chelating ligands," *J. Colloid Interface Sci.*, vol. 367, no. 1, pp. 139-147, 2012, doi: 10.1016/j.jcis.2011.10.021.

[15] F. Wu, Z. Wang, X. Li, and H. Guo, "Simple preparation of petal-like TiO2 nanosheets as anode materials for lithium-ion batteries," *Ceram. Int.*, vol. 40, no. PB, pp. 16805-16810, 2014, doi: 10.1016/j.ceramint.2014.07.060.

[16] X. Lü, F. Huang, J. Wu, S. Ding, and F. Xu, "Intelligent hydrated-sulfate template assisted preparation of nanoporous TiO2 spheres and their visible-light application," *ACS Appl. Mater. Interfaces*, vol. 3, no. 2, pp. 566-572, 2011, doi: 10.1021/am101137w.

[17] X. Lü, S. Ding, Y. Xie, and F. Huang, "Non-aqueous preparation of high-crystallinity hierarchical TiO2 hollow spheres with excellent photocatalytic efficiency," *Eur. J. Inorg. Chem.*, no. 18, pp. 2879-2883, 2011, doi: 10.1002/ejic.201100151.

[18] F. Di Lupo *et al.*, "Mesoporous TiO2 nanocrystals produced by a fast hydrolytic process as high-rate long-lasting Li-ion battery anodes," *Acta Mater.*, vol. 69, pp. 60-67, 2014, doi: 10.1016/j.actamat.2014.01.057.

[19] S. Casino, F. Di Lupo, C. Francia, A. Tuel, S. Bodoardo, and C. Gerbaldi, "Surfactant-assisted sol gel preparation of high-surface area mesoporous TiO2 nanocrystalline Li-ion battery anodes," *J. Alloys Compd.*, vol. 594, pp. 114-121, 2014, doi: 10.1016/j.jallcom.2014.01.111.

[20] S. Fang, L. Shen, Z. Tong, H. Zheng, F. Zhang, and X. Zhang, "Si nanoparticles encapsulated in elastic hollow carbon fibres for Li-ion battery anodes with high structural stability," *Nanoscale*, vol. 7, no. 16, pp. 7409-7414, 2015, doi: 10.1039/c5nr00132c.

[21] S. Wang, Y. Xing, C. Xiao, X. Wei, H. Xu, and S. Zhang, "Hollow carbon-shell/carbon-nanorod arrays for high performance Li-ion batteries and supercapacitors," *RSC Adv.*, vol. 5, no. 11, pp. 7959-7963, 2015, doi: 10.1039/c4ra14683b.

[22] T. Xia *et al.*, "Amorphous carbon-coated TiO2 nanocrystals for improved lithium-ion battery and photocatalytic performance," *Nano Energy*, vol. 6, pp. 109-118, 2014, doi: 10.1016/j.nanoen.2014.03.012.

[23] V. Etacheri, J. E. Yourey, and B. M. Bartlett, "Chemically bonded TiO2-Bronze nanosheet/reduced graphene oxide hybrid for high-power lithium ion batteries," *ACS Nano*, vol. 8, no. 2, pp. 1491-1499, 2014, doi: 10.1021/nn405534r.

[24] X. Lü *et al.*, "Enhanced electron transport in Nb-doped TiO2 nanoparticles via pressure-induced phase transitions," *J. Am. Chem. Soc.*, vol. 136, no. 1, pp. 419-426, 2014, doi: 10.1021/ja410810w.

[25] Y. X. Wang, J. Xie, G. S. Cao, T. J. Zhu, and X. B. Zhao, "Electrochemical performance of TiO 2/carbon nanotubes nanocomposite prepared by an in situ route for Li-ion batteries," *J. Mater. Res.*, vol. 27, no. 2, pp. 417-423, 2012, doi: 10.1557/jmr.2011.406.

[26] X. Lü *et al.*, "Improved-Performance Dye-Sensitized solar cells using Nb-Doped TiO 2 electrodes: Efficient electron Injection and transfer," *Adv. Funct. Mater.*, vol. 20, no. 3, pp. 509-515, 2010, doi: 10.1002/adfm.200901292.

[27] D. Liu *et al.*, "TiO2 nanotube arrays annealed in CO exhibiting high performance for lithium ion intercalation," *Electrochim. Acta*, vol. 54, no. 27, pp. 6816-6820, 2009, doi: 10.1016/j.electacta.2009.06.090.

[28] N. A. Kyerematen *et al.*, "Effect of Sn-doping on the electrochemical behaviour of TiO2 nanotubes as potential negative electrode materials for 3D Li-ion micro batteries," *J. Power Sources*, vol. 224, pp. 269-277, 2013, doi: 10.1016/j.jpowsour.2012.09.104.

[29] J. H. Jeong, D. W. Jung, E. W. Shin, and E. S. Oh, "Boron-doped TiO2 anode

materials for high-rate lithium ion batteries," *J. Alloys Compd.*, vol. 604, pp. 226-232, 2014, doi: 10.1016/j.jallcom.2014.03.069.

[30] G. Hasegawa, T. Sato, K. Kanamori, K. Nakanishi, and T. Abe, "Synthesis and electrochemical performance of hierarchically porous N-doped TiO2 for Li-ion batteries," *New J. Chem.*, vol. 38, no. 4, pp. 1380-1384, 2014, doi: 10.1039/c3nj01332d.

[31] Y. Zhou, Q. Bao, L. A. L. Tang, Y. Zhong, and K. P. Loh, "Hydrothermal dehydration for the 'green' reduction of exfoliated graphene oxide to graphene and demonstration of tunable optical limiting properties," *Chem. Mater.*, vol. 21, no. 13, pp. 2950-2956, 2009, doi: 10.1021/cm9006603.

[32] S. Chen, W. Chu, Y. Y. Huang, X. Liu, and D. G. Tong, "Preparation of porous nitrogen-doped titanium dioxide microspheres and a study of their photocatalytic, antibacterial and electrochemical activities," *Mater. Res. Bull.*, vol. 47, no. 12, pp. 4514-4521, 2012, doi: 10.1016/j.materresbull.2012.09.031.

[33] K. El Ouardi *et al.*, "Facile synthesis of nanoparticles titanium oxide as high-capacity and high-capability electrode for lithium-ion batteries," *J. Appl. Electrochem.*, vol. 50, pp. 583-595, 2020, doi: 10.1007/s10800-020-01419-y.

[34] M. Buaki-Sogo, M. Serra, A. Primo, M. Alvaro, and H. Garcia, "Alginate as Template in the Preparation of Active Titania Photocatalysts," *ChemCatChem*, vol. 5, no. 2, pp. 513-518, 2013, doi: 10.1002/cctc.201200386.

[35] J. Wang, Y. Zhou, B. Xiong, Y. Zhao, X. Huang, and Z. Shao, "Fast lithium-ion insertion of TiO2 nanotube and graphene composites," *Electrochim. Acta*, vol. 88, pp. 847-857, 2013, doi: 10.1016/j.electacta.2012.10.010.

[36] H. Cao, B. Li, J. Zhang, F. Lian, X. Kong, and M. Qu, "Synthesis and superior anode performance of TiO 2@ reduced graphene oxide nanocomposites for lithium ion batteries," *J. Mater. Chem.*, vol. 22, no. 19, pp. 9759-9766, 2012, doi: 10.1039/c2jm00007e.

[37] J. S. Chen, Y. L. Tan, C. M. Li, Y. L. Cheah, and D. Luan, "Ja100102Y.Pdf," no. 001, pp. 6124-6130, 2010.

[38] J. Wang, Y. Bai, M. Wu, J. Yin, and W. F. Zhang, "Preparation and electrochemical properties of TiO2 hollow spheres as an anode material for lithium-ion batteries," *J. Power Sources*, vol. 191, no. 2, pp. 614-618, 2009, doi: 10.1016/j.jpowsour.2009.02.056.

[39] A. K. Rai *et al.*, "Simple synthesis and particle size effects of TiO2 nanoparticle anodes for rechargeable lithium ion batteries," *Electrochim. Acta*, vol. 90, pp. 112-118, 2013, doi: 10.1016/j.electacta.2012.11.104.

[40] M. Das *et al.*, "One step hydrothermal synthesis of a rGO-TiO2 nanocomposite and its application on a Schottky diode: Improvement in device performance and transport properties," *RSC Adv.*, vol. 5, no. 123, pp. 101582-101592, 2015, doi: 10.1039/c5ra17795b.

[41] J. Ma *et al.*, "Lithium Intercalation in Anatase Titanium Vacancies and the Role of Local Anionic Environment," *Chem. Mater.*, vol. 30, no. 9, pp. 3078-3089, 2018, doi: 10.1021/acs.chemmater.8b00925.

[42] R. Fernández Acosta, E. Peláe Abellán, J. R. Correa, and U. Jáuregui Haza, "Nanostructured TiO2 Obtained by Electrolysis and its Application in the Remediation of Water Polluted with Paracetamol," *Int J Chem Mater Env. Res*, vol. 3, no. 2, pp. 20-28, 2016.

[43] A. Bhaumik and S. Inagaki, "Mesoporous titanium phosphate molecular-sieves with ion-exchange

capacity," *J. Am. Chem. Soc.*, vol. 123, no. 4, pp. 691-696, 2001, doi: 10.1021/ja002481s.

[44] R. Sasikala *et al.*, "Enhanced photocatalytic activity of indium and nitrogen co-doped TiO2-Pd nanocomposites for hydrogen generation," *Appl. Catal. A Gen.*, vol. 377, no. 1-2, pp. 47-54, 2010, doi: 10.1016/j.apcata.2010.01.039.

[45] X. Wang, Z. Hu, Y. Chen, G. Zhao, Y. Liu, and Z. Wen, "A novel approach towards high-performance composite photocatalyst of TiO 2 deposited on activated carbon," *Appl. Surf. Sci.*, vol. 255, no. 7, pp. 3953-3958, 2009, doi: 10.1016/j.apsusc.2008.10.083.